Talanta 230 (2021) 122276

Contents lists available at ScienceDirect

Talanta

journal homepage: www.elsevier.com/locate/talanta

Construction of a ternary nano-architecture based graphene oxide sheets, toward electrocatalytic determination of tumor-associated anti-p53 autoantibodies in human serum

Bahareh Feyzi-barnaji [a], Rassoul Dinarvand [a,b], Hamid Salehzadeh [c], Elham Arkan [d], Abdollah Salimi [e], Fatemeh Nili [f], Ali Mohammadi [b,g,*]

[a] Department of Pharmaceutical Nanotechnology, Faculty of Pharmacy, Tehran University of Medical Sciences, Tehran, Iran
[b] Nanotechnology Research Centre, Faculty of Pharmacy, Tehran University of Medical Sciences, Tehran, Iran
[c] Faculty of Chemistry, Kharazmi University, Tehran, 1571914911, Iran
[d] Nano Drug Delivery Research Center, Kermanshah University of Medical Sciences, Kermanshah, Iran
[e] Department of Chemistry, University of Kurdistan, 66177-15175, Sanandaj, Iran
[f] Department of Pathology, Imam Khomini Hospital Complex, Tehran University of Medical Sciences, Tehran, Iran
[g] Department of Drug and Food Control, Faculty of Pharmacy, Tehran University of Medical Sciences, Tehran, Iran

ARTICLE INFO

Keywords:
Electrochemical biosensor
Graphene oxide
$Ni(OH)_2$ nanoparticles
Horseradish peroxidase
anti-p53 autoantibody

ABSTRACT

Almost 13% of all death in the world is related to cancer. One of the major reasons for failing cancer treatment is the late diagnosis of the tumors. Thus, diagnosis at the early stages could be vital for the treatment. Serum autoantibodies, as tumor markers, are becoming interesting targets due to their medical and biological relevance. Among them, anti-p53 autoantibody in human sera is found to be involved in a variety of cancers. Regarding this issue, a novel and sensitive electrochemical biosensor for detection of anti-p53 autoantibody has been developed. For this purpose, a nanocomposite including thionine (as an electron transfer mediator)/chitosan/nickel hydroxide nanoparticles/electrochemically reduced graphene oxide (Th-CS-Ni$(OH)_2$NPs–ERGO) as a support platform was fabricated on the surface of glassy carbon electrode via a layer-by-layer manner and characterized through common electrochemical and imaging techniques. Then, p53-antigen was immobilized on the nanocomposite and used in an indirect immunoassay with horseradish peroxidase (HRP)-conjugated secondary antibody and H_2O_2 as the substrate, following the typical Michaelis–Menten kinetics. Under optimized condition, two techniques, including differential Pulse Voltammetry (DPV) and Electrochemical Impedance Spectroscopy (EIS) as a label free technique, applied for the biomarker detection. The linear ranges and LODs were obtained 0.1–500 pg mL^{-1} and 0.001 pg mL^{-1} using DPV and 5–150 pg mL^{-1} and 0.007 pg mL^{-1} using EIS, respectively. Furthermore, the proposed biosensor displayed satisfying stability, selectivity, and reproducibility. According to the results, the presented protocol is promising to develop other electrochemical biosensors.

1. Introduction

Cancer, also called malignancy, is an abnormal development of cells and the second cause of death after heart disease [1]. Mutation and genomic instability result in cancerous cells [2]. One of the most common mutation is related to the p53 gene, which causes the secretion of the anti-p53 autoantibody in the human serum before the onset of the clinical symptoms of cancer [1]. So, anti-p53 autoantibody has been expressed in various malignancies such as liver [3], ovarian [4], breast [5], lung [6], and esophageal [7]. Several traditional methods including enzyme-linked immunosorbent assay (ELISA) [8], electrochemiluminescence (ECL) [9], and Western blot [10] have been applied for quantification of anti-p53 autoantibody. However, the drawbacks of these complicated procedures, such as low sensitivity and high cost, limit the wide-spreading application of these methods. Furthermore, most of these methods provide qualitative or semi-quantitative outputs [11]. On the other hand, implementation of the electrochemical methods in the clinical analysis could potentially give us a rapid, specific, inexpensive, and fully automated means of biomarker analysis [12].

* Corresponding author. Nanotechnology Research Centre, Faculty of Pharmacy, Tehran University of Medical Sciences, Tehran, Iran.
E-mail address: alimohammadi@tums.ac.ir (A. Mohammadi).

https://doi.org/10.1016/j.talanta.2021.122276
Received 4 January 2021; Received in revised form 25 February 2021; Accepted 1 March 2021
Available online 19 March 2021

Recently, various electrochemical biosensors have developed for anti-p53 autoantibody detection [1,13,14]. Reda Elshafey and co-workers fabricated a biosensor for anti-p53 autoantibody detection at concentration range 0.1 pg mL^{-1} to 10 ng mL^{-1}, using AuNPs assembled onto the reduced graphene oxide (RGO) on a screen printed carbon electrode (SPCE) [1]. In addition, Garranzo-Asensio et al. developed an electrochemical biosensor based on conjugating MBs with HaloTag fusion p53 protein for capturing anti-p53 autoantibody and electro-reduction of hydroquinone (HQ) which produces from the HRP-enzymatic oxidation process. The dynamic range and LOD were found 1.1–5 U/mL and 0.34 U/mL, respectively [15]. In another report, the gold loaded nanoporous ferric oxide nanocubes with HRP-like activity have been used for developing of an amperometric and colorimetric biosensor for detection of anti-p53 autoantibody. The limit of detection for the colorimetric and amperometric assay were 0.12 U mL^{-1} and 0.08 U mL^{-1}, respectively [11].

Due to the unique properties of nanomaterials such as large surface area, biocompatibility and stability, application of various nano-structured materials for development of electrochemical biosensors has attracted great interest [16–18]. Between different nanomaterials, graphene oxide (GO) and reduced graphene oxide (RGO) have been widely utilized in neurobiology (drug delivery and tissue engineering), gas separation, biosensing, bio-imaging, electrochemical sensing, and photo-thermal therapy [19,20]. Integration of other nanomaterials such as metal nanoparticles or other organic molecules with RGO, may further improve its conductivity. Over the recent years, nano-composites based on GO or RGO were functionalized with nano-particles due to synergistic effect of combination of graphene-metal nanoparticles for fabrication of various nanosensors have been reported [21–23]. For example, Atar and coworkers used Fe@Ag nano-particles decorated reduced graphene oxide as an improved anode material for lithium-ion batteries fabrication [24]. In addition, Mehmet Lutfi Yola and coworker reported a nanosensor based on Ru@Au core-shell nanoparticles involved in carbon nitride nanotubes functionalized graphene quantum dots for phenylethanolamine detection [25].

$Ni(OH)_2$ NPs, a typical lamellar-type hydroxide, have gained attention due to the low cost, high electro-catalytic activity, and significant theoretical capacity [26]. On the other hand, chitosan (CS), a natural nontoxic biopolymer contains reactive amino and hydroxyl functional groups, which is applied widely in nano medicine due to its low cost, biodegradability, biocompatibility, film-forming ability, good adhesion, high water permeability and antimicrobial activities [27–29].

In addition, the presence of reactive amine or hydroxyl functional groups in CS showed a great property to chemical modification and also coordinate to the transition metal or their stabilization. Considering the specific ability of CS as immobilizing matrix, detecting elements such as antibodies or other proteins can be immobilized on to the CS backbone with covalent bonding [30,31]. Due to its poor conductivity, CS is usually combined with some carbonaceous nanomaterials, metal nano-particles, and redox mediators such as methylene blue [29] or thionine [32] for developing electrochemical biosensing platforms. So, the integration of CS, nanomaterials and redox mediators may provide a remarkable synergistic augmentation of electrochemical biosensors performance [32].

The current report describes designing of an anti-p53 autoantibody electrochemical biosensor based on ERGO decorated $Ni(OH)_2$NPs and CS nanocomposite modified electrode as a supporting matrix for covalent attachment of p53-antigen and thionine (Th) as electron transfer mediator. We used an indirect immunoassay with HRP-conjugated secondary antibody and H_2O_2 as the substrate for determination of anti-p53 autoantibody. The prepared CS/Ni $(OH)_2$ NPs/ERGO nanocomposite was characterized by Atomic Force Microscopy (AFM), Field Emission Scanning Electron Microscopy (FESEM), Energy Dispersive X-ray Spectroscopy (EDS), electrochemical impedance spectroscopy (EIS), and cyclic voltammetry (CV) techniques. For anti-p53 autoantibody quantification, both Differential Pulse Voltammetry (DPV) and EIS as analytical methods were applied. In addition, parameters including pH effect, incubation time, Th concentration, number of cycles for Th electrodeposition, and demanded H_2O_2 concentration have been optimized. Stability and reproducibility of the biosensor were also evaluated. Also, the selectivity of the biosensor was tested under the same experimental conditions, by challenging the biosensor against anti-p53 autoantibody in the presence of other antibodies including anti-HSA antibody, anti-AFP antibody, anti-PSA antibody, and anti-CEA antibody as interference agents. Finally, the clinical applicability of the prepared biosensor has been examined for detecting anti-p53 autoantibody in serum samples obtained from healthy and cancerous subjects. Since the prepared platform possess high enzymatic-activity towards catalytic oxidation of Th in the presence of H2O2, it is envisaged that the proposed bioassay could meet a wide range of application in the field of bioanalysis and clinical diagnostics.

2. Experimental

2.1. Chemical and reagents

Highly purified human p53-antigen, anti-p53 autoantibodies, and HRP-conjugated anti-human IgG (goat) as secondary antibody were purchased from R&D systems and abcam. Graphene oxide Nanoplatelet (99+%, 3.4–7 nm, 6–10 layers) was obtained from US Research Nanomaterials, Inc., USA. $K_3Fe(CN)_6$ and $K_4Fe(CN)_6$, nickel nitrate ($Ni(NO_3)_2$), chitosan, thionine, potassium chloride, acetic acid (AA) and sodium acetate, Bovine Serum Albumin (BSA) and all other reagents with analytical grade were received from Sigma-Aldrich company. Phosphate Buffer Saline (PBS) solution with pH = 7.4 was used for all electrochemical analysis and performed at room temperature 25 ± 0.1 °C.

2.2. Apparatus and procedures

The electrochemical experiments were carried out using a computer-controlled potentiostat, Autolab analyzer model PGSTAT30 (Eco Chemie, Utrecht, The Netherlands) driven with GPES software, and a μ-AutolabIII/FRA2 potentiostat/galvanostat coupled with NOVA 1.11 software in conjunction with a traditional three electrode system. A glassy carbon disc (1.8 mm diameter), a saturated calomel electrode (SCE) and a platinum wire were used as bare working, reference and counter electrodes, respectively. Due to data storage and processing, the whole system was connected to a personal computer. The nature and morphology of the prepared nanomaterials were characterized via SEM and TEM techniques.

2.3. Preparation of the modified electrode

Uniform GO dispersion (1 mg ml^{-1}) was achieved in bidistilled water by ultrasonication of the dispersion in an ultrasonic bath for 30 min. Prior to the modification, the GCE was polished first with alumina slurry on a polishing cloth, rinsed thoroughly twice with bidistilled water and then sonicated in bidistilled water/ethanol solution for 60 s. Two microliters of dispersed GO has been drop-casted on a GC electrode and dried at room temperature. The reduced form of GO was obtained by applying a constant potential of −1.3 V for 500 s in acetate buffer solution (pH = 5.0) while bubbling N_2 gas, resulting a stable film of ERGO (electrochemically reduced graphene oxide) on the GC electrode. Hereafter, the fabricated electrode was denoted as ERGO/GCE. An elegant approach of in situ electrodeposition technique was used for the synthesis of $Ni(OH)_2$ NPs on the ERGO/GCE surface. Electrochemical in situ deposition from a degassed acetate buffer solution (pH = 5.0), containing 1 mM nickel nitrate has been performed on the ERGO/GCE

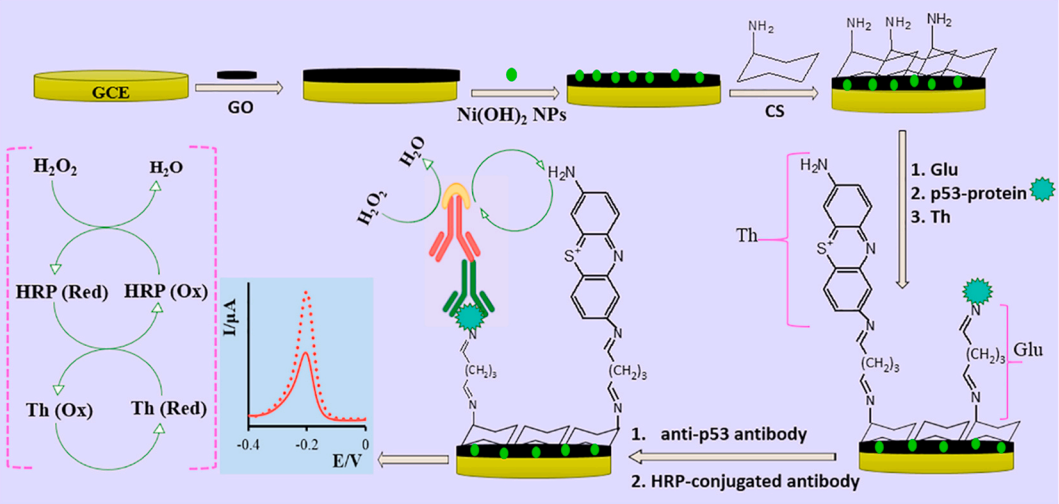

Scheme 1. Schematic illustration for the fabrication of the anti-p53 autoantibody biosensor.

by application of a constant potential of 1.0 V (vs. SCE) for 100 s. This step was followed by immersion of the electrode in a 0.1 M NaOH solution. Afterward, electro-dissolution of the nickel oxide layer and the growth of nickel hydroxide film were performed by consequence potential cycling in a potential window of −0.5 to +0.8 V at a scan rate of 100 mV s^{-1} [33,34]. This modified electrode was denoted as $Ni(OH)_2$ NPs/ERGO/GCE. Then, 2 μL of the prepared chitosan solution (1 mg in 10 mL acetic acid 0.1 M) was dropped on the $Ni(OH)_2$NPs/ERGO/GCE surface. After evaporation of the solvent, the electrode surface was rinsed with bidistilled water to wash away the un-immobilized modifier and dried at room temperature. The resulting electrode was denoted as CS/$Ni(OH)_2$ NPs/ERGO/GCE.

2.4. Fabrication of the biosensor and anti-p53 autoantibody detection

The modified electrode (CS/$Ni(OH)_2$ NPs/ERGO/GCE) was immersed in glutaraldehyde (Glu) solution (%0.3) as a linker for 60 min. After rinsing the fabricated electrode with bidistilled water, the biosensor (p53-antigen/Glu/CS/$Ni(OH)_2$NPs/ERGO/GCE) was assembled by immobilizing 5 μL p53-antigen (50 ng mL^{-1}) onto the prepared electrode overnight at 4 °C in a moist condition. Thereafter, 0.1 mM Th in phosphate buffer (pH = 6.5) was electrodeposited on the modified electrode by 20 consequence potential cycling at potential window +0.5 to −0.7 V at a scan rate of 100 mVs^{-1}. After rinsing the modified electrode with bidistilled water, it can be used for further experiments or stored at the moist condition when not in use. Afterward, the fabricated electrode was washed with PBS to remove unbounded proteins, and Th, and then 10 μL of BSA (5%) in the PBS was added to block the residual active sites of Glu and avoid non-specific binding. The biosensor was denoted as Th/p53-antigen/CS/$Ni(OH)_2$ NPs/ERGO/GCE. The designed biosensor was stored at 4 °C when not in use under buffer humidity. As shown in Scheme 1, both p53-antigen and Th are covalently attached onto $-NH_2$ functional groups of CS. In order to quantification of anti-p53 autoantibody, the biosensor was incubated in different concentration of anti-p53 autoantibody at room temperature for 50 min. At the next step, 10 μl of HRP-conjugated secondary antibody (20 ng mL^{-1}) was loaded onto the biosensor surface and incubated for 60 min at room temperature. The biosensor was washed thoroughly with PBS and placed into the 2.5 mM H_2O_2 solution. The anti-p53 autoantibody quantification was carried out by measuring the thionine peak current in the presence of H_2O_2. The biosensor was called HRP-labeled secondary antibody/anti-p53 autoantibody/Th/p53-antigen/CS/$Ni(OH)_2$ NPs/ERGO/GCE. The biosensor fabrication steps are shown in Scheme 1.

3. Results and discussion

3.1. Electrode surface characterization

Surface morphology of the ERGO was observed by the field emission scanning electron microscope (FESEM). As illustrated in Fig. 1A, ERGO nanosheets consist of wrinkled surface morphology and aggregated randomly. Moreover, isolated $Ni(OH)_2$ NPs were deposited uniformly on the surface of ERGO/GC electrode by electrochemical reduction of nickel ions (Fig. 1B). Fig. 1C obviously indicates that the morphology of the modified electrode surface (CS/Ni$(OH)_2$ NPs/ERGO/GCE) was changed after drop-casting of the CS on the $Ni(OH)_2$ NPs/ERGO/GCE surface. Such an excellent surface area obtained by distribution of the $Ni(OH)_2$ NPs on the ERGO layer and drop-casting of CS, helped to the performance of modified electrode. In order to obtain topographical information and surface roughness, the modified electrodes were analyzed by AFM and paired with their corresponding FESEM micrographs in Fig. 1. The micrographs of the ERGO, $Ni(OH)_2$ NPs/ERGO and CS/$Ni(OH)_2$ NPs/ERGO modified electrodes represent surfaces with root mean square (RMS) roughness of 13.2, 15.4, and 65.1 nm, respectively. These results indicated that the roughness of the modified electrodes increased by stepwise modification.

To further demonstrate the successful GCE modification, the elementary composition of ERGO, $Ni(OH)_2$ NPs/ERGO, and CS/$Ni(OH)_2$ NPs/ERGO modified electrodes were analyzed via EDS technique. As depicted in Fig. 2, C, O, Ni, and N elements were detected on the surface of the modified electrodes, which confirmed the success of the modification processes.

3.2. Electrochemical characteristics of the modified electrode

3.2.1. Cyclic voltammetry

During preparation steps, the changes of the biosensor behavior were monitored by recording CVs from aqueous solution containing 5 mM $[Fe(CN)_6]^{-3/-4}$ redox couple system and 0.1 M KCl at a scan rate of 100 mV s^{-1}. As illustrated, a reversible redox couple at the bare GCE was observed (Fig. 3A, voltammogram "a"). After drop-casting of GO, the electron transfer rate of the modified electrode due to the presence of oxy groups on the surface of GO nanosheets were decreased, which leads to a reduction in the current response at the GO/GCE surface [35]. However, the current was greatly increased after electro-reduction of GO, indicating large effective surface area and excellent electrical features of ERGO (Fig. 3A, voltammogram "b"). Meanwhile, $Ni(OH)_2$ NPs exhibit excellent

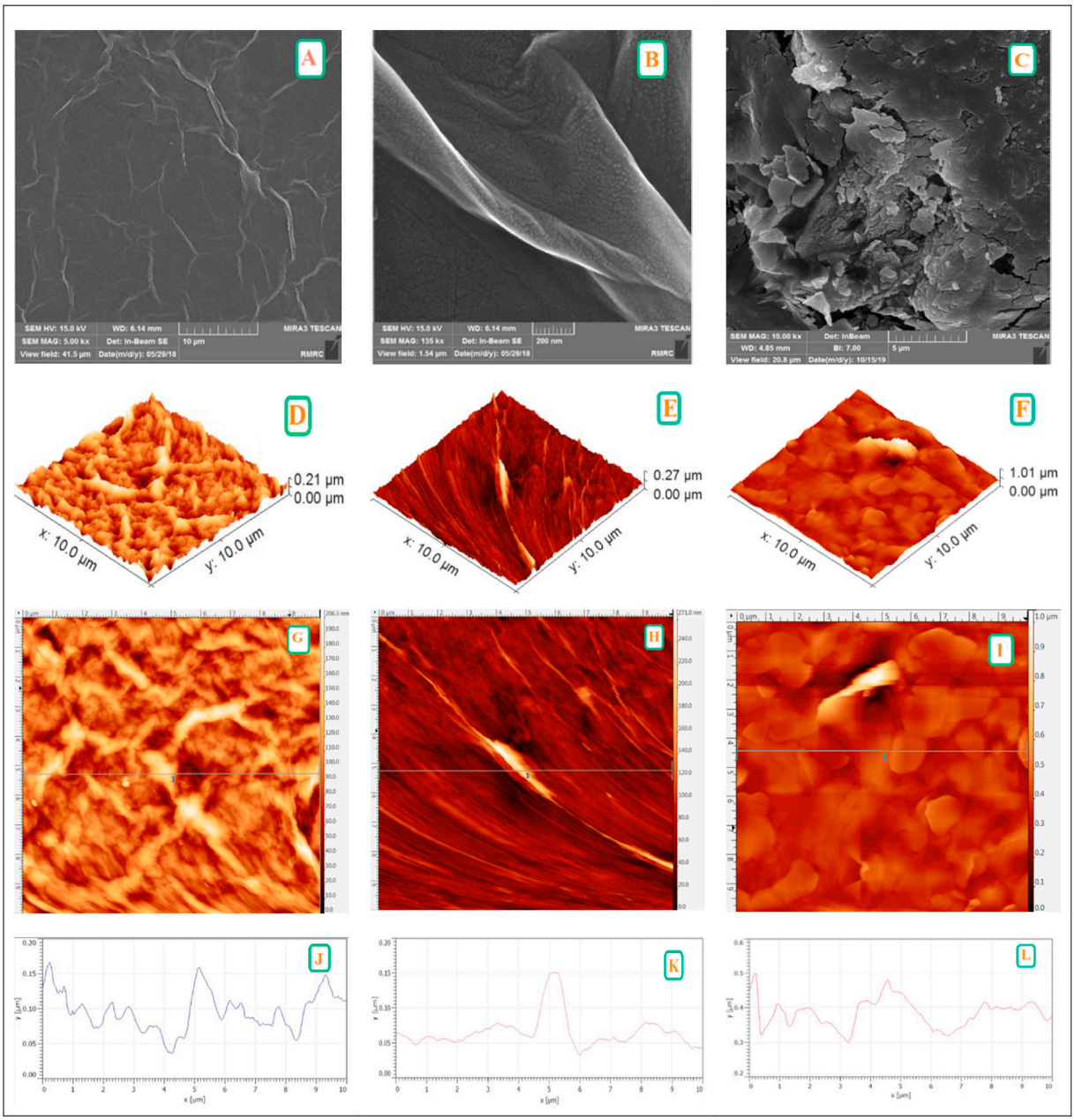

Fig. 1. FESEM micrographs of (A) GO/GCE, (B) $Ni(OH)_2$NPs/ERGO/GCE, and (C) CS/$Ni(OH)_2$NPs/ERGO/GCE. AFM micrographs of (E) GO/GCE, (F) $Ni(OH)_2$ NPs/ERGO/GCE, and (G) CS/$Ni(OH)_2$ NPs/ERGO/GCE.

electrochemical performance due to their high surface area as well as a large number of adsorptive sites, causing enhancement of the response (Fig. 3A, voltammogram "c"). Additionally, the response was further increased at the CS/$Ni(OH)_2$ NPs/ERGO/GC modified electrode due to the presence of the positively charged groups of CS, which facilitated diffusion of $[Fe(CN)6]^{-3/-4}$ (as an anion) through the modified electrode surface (Fig. 3A, voltammogram "d"). The reduction of the peak current after attachment of Glu onto the modified electrode (Fig. 3A, voltammogram "e") confirms the formation of a film layer of Glu on the surface of the modified electrode. After immobilization of 5 µL p53-antigen (50 ng mL^{-1}), due to resistance toward electron transfer, a dramatic decrease in the response was observed (Fig. 3A, voltammogram "f"). Afterward, anti-p53 autoantibody/p53-antigen immuno-complex was formed by interaction of anti-p53 autoantibody with the surface of the p53-antigen/Glu/CS/$Ni(OH)_2$NPs/ERGO/GCE. As expected, the current response of the probe was further decreased (voltammogram "g"), demonstrating that the immuno-complex acts as a blocking layer and hinders the diffusion of ferricyanide ions toward the surface of the modified electrode [36]. As portrayed in Fig. 3A, voltammogram "h", the redox peak current of $[Fe(CN)6]^{-3/-4}$ at the surface of HRP-conjugated secondary antibody/anti-p53 autoantibody/BSA/p53-antigen/Glu/CS/$Ni(OH)_2$NPs/ERGO/GCE was lower than that of the anti-p53 autoantibody/BSA/p53-antigen/Glu/CS/$Ni(OH)_2$NPs/ERGO/GCE. This behavior demonstrates that the electron transfer was further hindered by the presence of these proteins. On the other hand, the surface areas of the electrodes, including bare GC, ERGO, $Ni(OH)_2$NPs/ERGO, CS/$Ni(OH)_2$NPs/ERGO, Glu/CS/$Ni(OH)_2$NPs/ERGO, p53-antigen/Glu/CS/$Ni(OH)_2$NPs/ERGO, anti-p53 autoantibody/BSA/p53-antigen/Glu/CS/$Ni(OH)_2$NPs/ERGO, and HRP-conjugated secondary antibody/anti-p53 autoantibody/BSA/p53-antigen/Glu/CS/$Ni(OH)_2$NPs/ERGO modified electrodes were calculated using Randles-Sevcik equation [35](Fig. 3A, inset). As expected, the results indicated that surface area of the modified

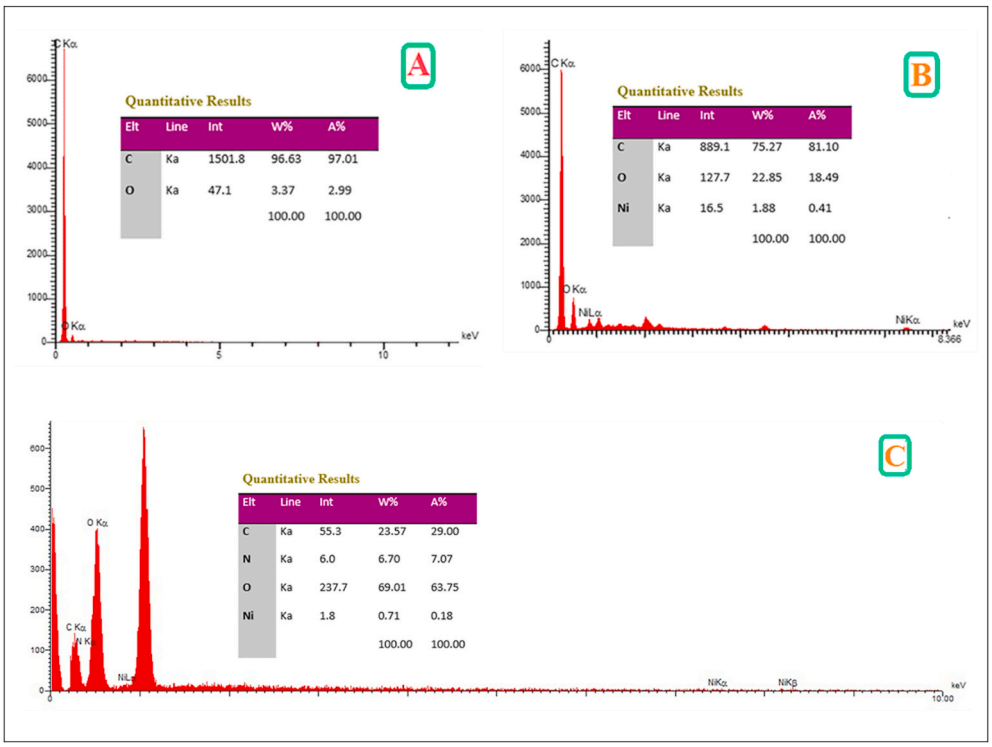

Fig. 2. EDS spectra of different electrodes: (A) ERGO/GCE, (B) $Ni(OH)_2$NPs/ERGO/GCE, and (C) CS/$Ni(OH)_2$ NPs/ERGO/GCE.

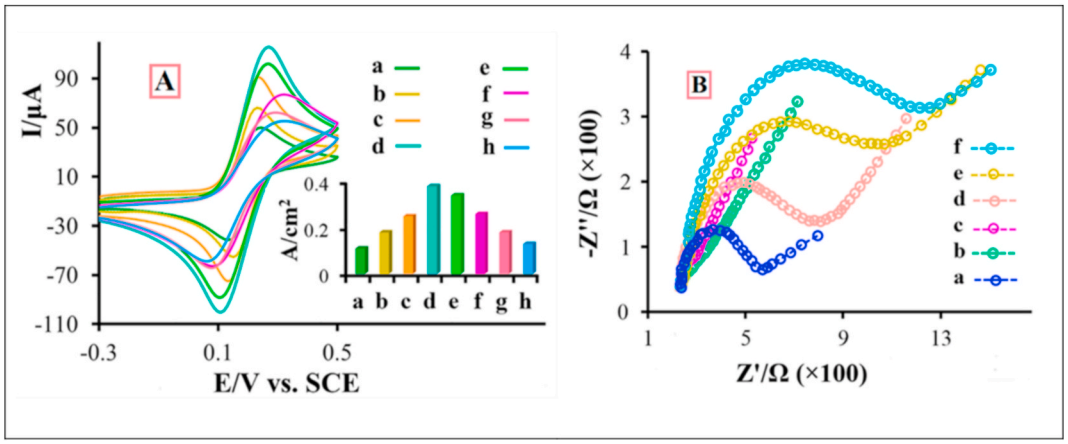

Fig. 3. (A) CVs (a) bare, (b) ERGO, (c) $Ni(OH)_2$ NPs/ERGO, (d) CS/$Ni(OH)_2$ NPs/ERGO, (e) Glu/CS/$Ni(OH)_2$ NPs/ERGO, (f) p53-antigen/Glu/CS/$Ni(OH)_2$NPs/ERGO, and (g) anti-p53 autoantibody/BSA/p53-antigen/Glu/CS/$Ni(OH)_2$ NPs/ERGO, and (h) HRP-conjugated secondary antibody/anti-p53 autoantibody/BSA/p53-antigen/Glu/CS/$Ni(OH)_2$NPs/ERGO modified GCEs and (B) EIS plots of (a) bare, (b) ERGO, (c) CS/$Ni(OH)_2$NPs/ERGO, (d) p53-antigen/Glu/CS/$Ni(OH)_2$NPs/ERGO, (e) anti-p53 autoantibody/BSA/p53-antigen/Glu/CS/$Ni(OH)_2$ NPs/ERGO, and (f) HRP-conjugated secondary antibody/anti-p53 autoantibody/BSA/p53-antigen/Glu/CS/$Ni(OH)_2$NPs/ERGO. The CVs and EISs recorded in 5 mM $[Fe(CN)_6]^{-3/-4}$ solution containing 0.1 M KCl at scan rate 100 mV s^{-1} and frequency range from 0.1 to 10 kHz, respectively.

electrodes increased step by step during modification process and then decreased in the presence of the proteins.

3.2.2. *Electrochemical impedance spectroscopy characterization*

The biosensor fabrication process steps has also evaluated using EIS. Fig. 3B represents the Nyquist plots of the unmodified and modified electrodes in the presence of 0.1 M KCl and 5 mM $[Fe(CN_6)]^{-3/-4}$ solution, at frequency range of 0.1 Hz–100 kHz. Fig. 3B plot "a" shows a large semicircular plot for unmodified GCE. Also, GO acts as an insulating film, showing a much larger semicircular than that of the bare GCE (data not shown). This behavior is attributed to the presence of oxy residues on the surface of GO. The plot of ERGO/GCE represents a straight line in the low frequency region, which is characteristic of the diffusion controlled electrochemical processes (Fig. 3B, plot "b"). This is due to the in situ elimination of unstable oxy groups upon electroreduction, leading significant improvement in the conduction pathways for charge transfer. In the meantime, CS/$Ni(OH)_2$ NPs/ERGO modified electrode exhibited very low resistance (Fig. 3B, plot "c"). These results imply that the proposed nanomaterials facilitated the electron transfer using supplying favorable conduction pathways and their synergistic effect. After immobilization of p53-antigen, the charge transfer resistance was drastically increased due to the presence of the hydrophobic layer of protein, which hindered the electron transfer at the modified electrode surface (Fig. 3B, plot "d"). When anti-p53

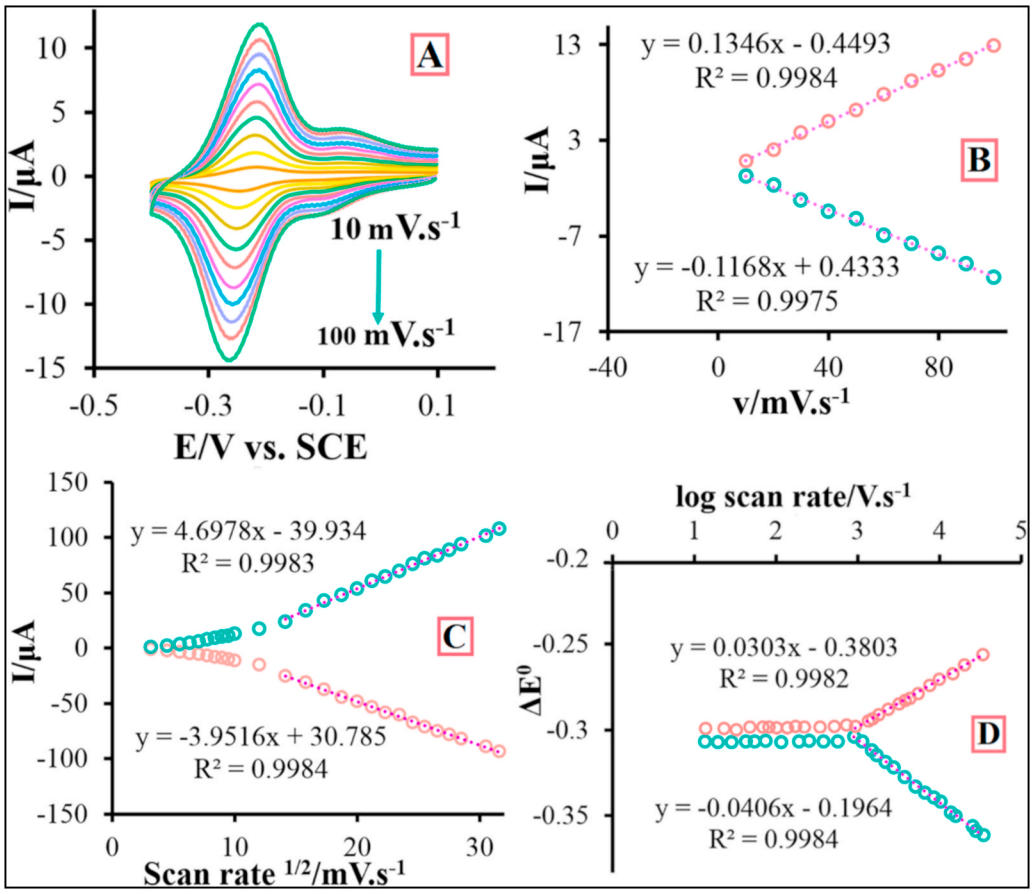

Fig. 4. CVs of electrodeposited Th in 0.1 M PBS (pH = 7.0) at (A) different scan rates from 10 to 100 mV s^{-1}. Plots of peak currents vs. (B) υ, (C) $\upsilon^{1/2}$, and (D) log υ.

autoantibody adsorbed, due to the formation of hydrophobic immunocomplex layer of the proteins, which perturbs the interfacial electron transfer, semicircular diameter was further increased (Fig. 3B, plot "e"). Finally, by loading HRP-conjugated secondary antibody on the prepared immunosensor surface, the semicircular diameter significantly increased (Fig. 3B, plot "f").

In addition, cyclic voltammetry was applied for the investigation of the electrodeposited $Ni(OH)_2$ layer on the bare and ERGO modified electrodes. To this purpose, the modified electrodes were immersed in the 0.1 M NaOH solution, and the CVs were recorded in the potential window from 0.2 to 0.55 V at a scan rate 100 mV s^{-1}. As depicted in the Fig. S1a, the recorded CV of Ni $(OH)_2$NPs/GCE shows a one anodic/cathodic peak pair at 0.48/0.42 V. The anodic peak is related to the oxidation of the $Ni(OH)_2$ phase to NiO(OH) at 0.48 V, and the NiO(OH) is reduced back to the $Ni(OH)_2$ upon a reduction peak at 0.42 V [33,37]. Furthermore, the recorded CV of the $Ni(OH)_2$NPs/ERGO/GC electrodes were displayed in the Fig. S1b. As seen, the current of the $Ni(OH)_2$NPs/ERGO/GCE was dramatically enhanced in comparison to the Ni $(OH)_2$NPs/GCE, indicating a larger surface area of the ERGO which increased number of electrodeposited $Ni(OH)_2$NPs on the surface of the ERGO/GCE.

3.2.3. Charge transfer study of the redox mediator

In Fig. 4A a reversible redox system is illustrated for the electrodeposited Th. As seen in Fig. 4B, the peak currents linearly increased with an increase in the scan rate from 10 to 100 mV s^{-1}. Moreover, plotting the anodic and cathodic peak currents vs. square root of the scan rate ($\upsilon^{1/2}$) exhibits good linearity showing diffusion-controlled electron transfer and also changing of ΔE_p value versus the logarithm of the scan rate is almost negligible, indicating a facile charge transfer kinetics over this range of scan rate, as presented in Fig. 4C and D, respectively. According to the Laviron theory [38], the charge transfer coefficient (α) and apparent charge transfer rate constant (k_s), of a surface confined redox compound can be determined by changing the variation of anodic and cathodic peak potentials against the logarithm of the scan rate into a trumpet-like shape (Fig. 4D). These parameters including α and k_s (for the cathodic branch) found to be 0.52 and 29.8 s^{-1}, respectively, suggesting that CS/$Ni(OH)_2$NPs/ERGO/GCE was capable of enhancing the electron transfer rate between electrode and Th interface.

3.3. Stability of the modified electrode

Stability evaluation is necessary for developing the bioassay method. The electrochemical stability of the modified electrode (Th/CS/$Ni(OH)_2$ NPs/ERGO/GCE) was checked by recording of repetitive CVs at a scan rate of the 100 mVs^{-1} in the PBS solution (pH = 7). As seen from Fig. S2, after 100 repetitive scans, no changes in the peak currents nor peak potential separation of CVs were observed. The stability of the biosensor was also investigated by storing at 4 °C in PBS (pH = 7) when not in use. To this purpose, different storage periods were utilized to detect the same concentration of anti-p53 autoantibodies. The biosensor retained 98.5% of its initial response after one-week storage and then started to decline to 94.2% after three weeks. Due to the high stability of Th/CS/Ni $(OH)_2$ NPs/ERGO layers and covalently immobilization of p53 proteins, the proposed biosensor is fairly stable.

3.4. The investigation of the enzyme electrocatalytic behavior

Horseradish peroxidase (HRP), a heme-containing peroxidase, is commonly used as an enzyme for fabricating electrocatalytic biosensors [39–41].

On the other hand, Th can catalyze the reduction of H_2O_2

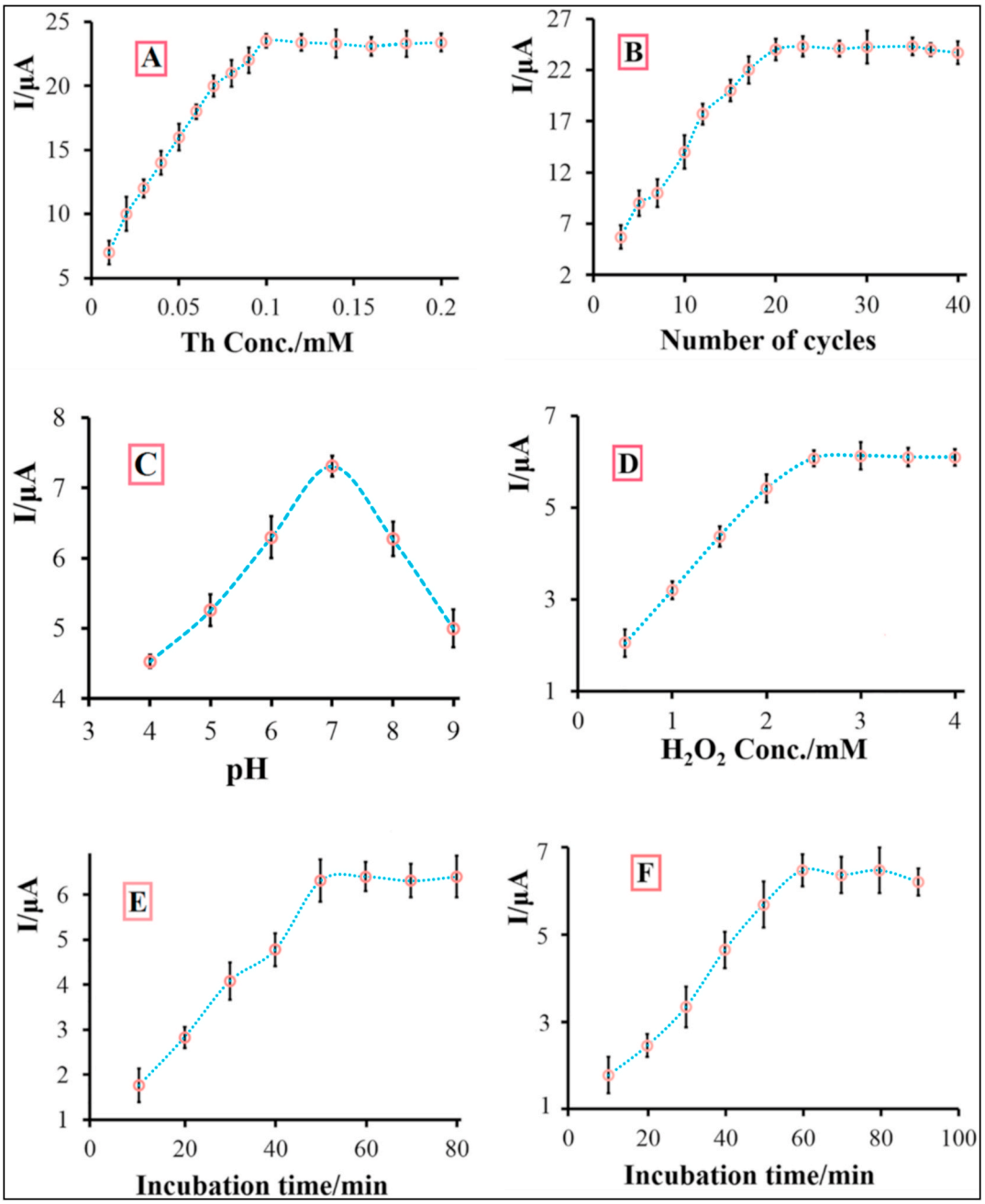

Fig. 5. Optimization of (A) Th concentration, (B) Number of cycles in Th electrodeposition, (C) effect of pH, (D) H_2O_2 concentration, (C) Th concentration (D) Scan number of Th electrodeposition, (E) Incubation time for p53-antigen and anti-p53 autoantibody interaction, and (f) Incubation time for anti-p53 autoantibody and HRP-conjugated secondary antibody interaction. Error bars indicate the standard deviation (SD) of three times measurements (n = 3).

through HRP [32]. As displayed in Fig. S3a, CV of Th in PBS containing 2.5 mM H_2O_2 shows two well-defined peaks at the surface of Th/p53-antigen/Glu/CS/ERGO/GCE. AS expected, there is no catalytic current for H_2O_2 reduction in the absence of anti-p53 autoantibody. These results are in good agreement with the previous studies [32,36]. When the biosensor incubated with 10 μL anti-p53 autoantibody (50 pg mL^{-1}) and 10 μL of 20 ng mL^{-1} HRP-conjugated secondary antibody, the current of oxidation peak decreased, while the current of reduction peak increased. This behavior is related to the electrocatalytic property of Th and HRP toward H_2O_2 reduction (Fig. S3b). As the concentration of anti-p53 autoantibody increased (100 pg mL^{-1}), the electrocatalytic current increasing (Fig. S3c). The results imply that Th can be the right choice as an electron transfer mediator, and HRP/Th couple shows appropriate electrocatalytic activity toward H_2O_2. The proposed mechanism presents the enzymatic catalytic reduction of H_2O_2 as follows [32]:

$$Thionine_{(ox)} + 2e^- \rightarrow Thionine_{(red)} \quad (1)$$

$$Thionine_{(red)} + HRP_{(ox)} \rightarrow HRP_{(red)} + Thionine_{(ox)} \quad (2)$$

$$HRP_{(red)} + H_2O_2 \rightarrow HRP_{(ox)} + H_2O \quad (3)$$

On the other hand, voltammogram "a" in Fig. S4 shows the response of 100 pg. mL^{-1} anti-p53 autoantibody at the surface of Th/p53-antigen/Glu/CS/Ni(OH)$_2$NPs/ERGO/GCE in the presence of PBS containing 2.5 mM H_2O_2 solution. When this modified electrode was incubated with 20 ng mL^{-1} HRP-conjugated secondary antibody (Fig. S4, voltammogram "b"), the current of the recorded DPV was

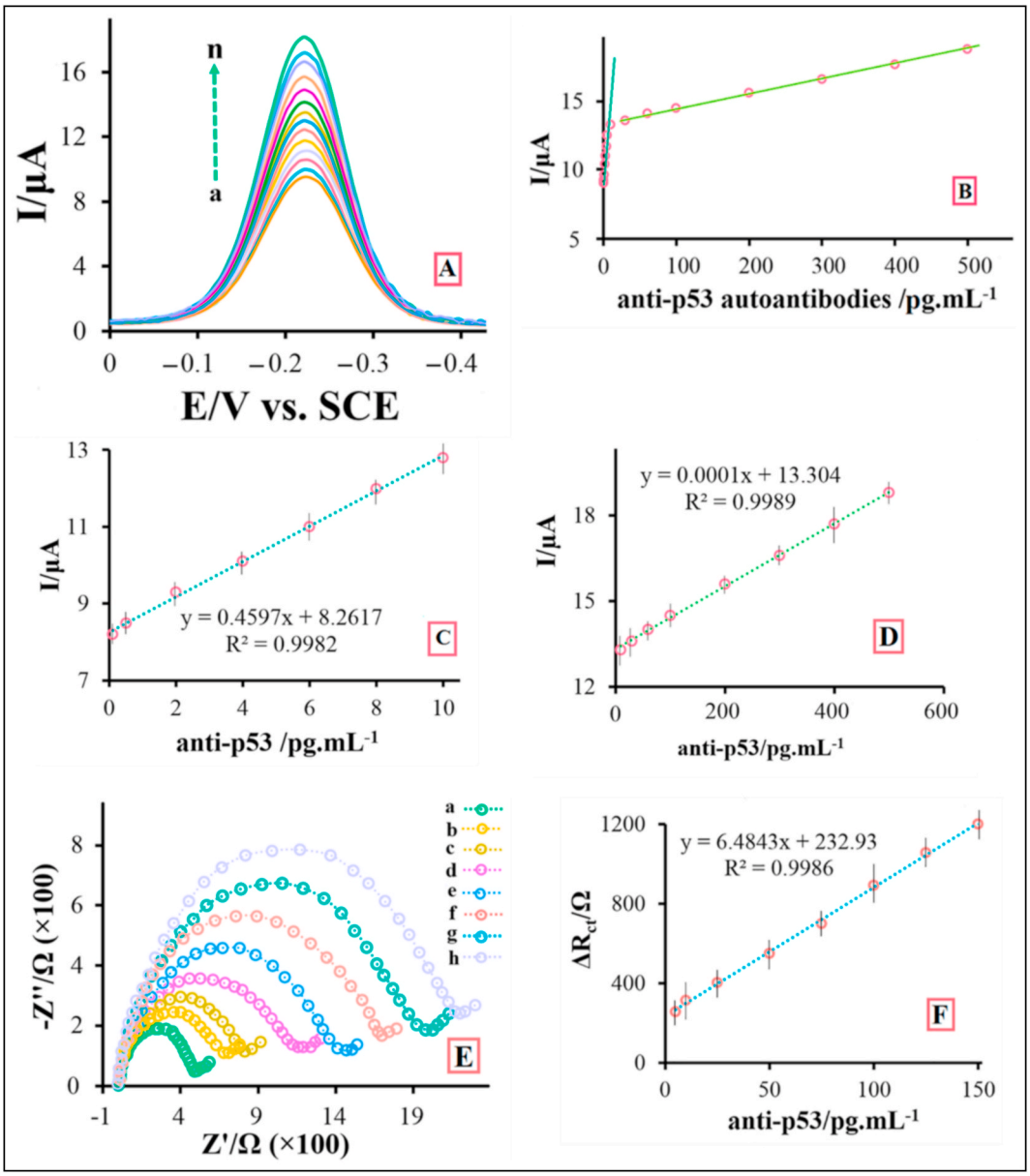

Fig. 6. (A) DPVs recorded in various concentrations of anti-p53 autoantibody in PBS (pH = 7.0) containing 2.5 mM H_2O_2, the arrow indicates increasing concentrations; (a) 0.1, (b) 0.5, (c) 2, (d) 4, (e) 6, (f) 8, (g) 10, (h) 30, (i) 60, (j) 100, (k) 200, (l) 300, (m) 400, and (n) 500 pg mL^{-1}.(B) Calibration curves based on resulted DPVs for anti-p53 autoantibody concentrations from 0.1 to 500 pg mL^{-1}; (C) for first linear range (0.1–10 pg mL^{-1}), and (D) for second linear range (10–500 pg mL^{-1}). (E) EIS plots obtained in different concentrations of anti-p53 autoantibody in $[Fe(CN)6]^{-3/-4}$ and 0.1 M KCl; (a) 5, (b) 10, (c) 25, (d) 50, (e) 75, (f) 100, (g) 125, and (h) 150 pg mL^{-1}. (F) Calibration curves based on resulted EISs for anti-p53 autoantibody concentrations from 5 to 150 pg mL^{-1}. Error bars indicate the standard deviation (SD) of three times measurements (n = 3).

increased. This behavior is attributed to the presence of HRP-conjugated secondary antibody and the electrocatalytic activity of the immobilized HRP toward H_2O_2 reduction. These results imply that the amplification effect obtained by the as-prepared biosensor.

3.5. Optimization of the analytical conditions

In an immunosensing assay, different parameters affect on the biosensor response, so the measuring carried out at optimum condition. To find the optimal condition for the best performance of the as-prepared biosensor, various parameters including Th concentration, the number of cycles for Th electrodeposition, effect of pH, p53-antigen concentration, incubation time between p53-antigen and anti-p53 autoantibody, concentration of H_2O_2, and incubation time between anti-p53 autoantibody with secondary antibody labeled with HRP should be optimized.

3.5.1. Th concentration

In order to achieve maximum performance of the biosensor, the effect of Th concentration on the biosensor performance was examined by immersing the CS/$Ni(OH)_2$NPs/ERGO/GC modified electrode in PBS solution (pH = 6.5) containing various concentrations of Th over the range from 0.01 to 0.2 mM and applying repetitive cycling at a potential window of −0.5 to +0.3 V at scan rate 100 mV s^{-1}. It is evident that as the Th concentration increases from 0.01 to 0.1 mM, the DPV current response increases accordingly, and then the peak current levels off for the higher concentration of Th (Fig. 5A). Thus, the optimal value of Th concentration was found to be 0.1 mM for the immunosensor fabrication.

3.5.2. Cycle numbers of Th electrodeposition

The effect of CV scan numbers was evaluated during the electrodeposition of Th on the surface of the modified electrode. Fig. 5B depicts an enhancement in the oxidation peak current of Th in parallel with increase of cycle numbers from 3 to 20, implying that Th was successfully deposited onto electrode surface. However, with increasing the cycle's number to 40, the peak current is nearly the same as that obtained for 20 scans. Applying redundant scans ultimately leads to side reactions occurring on the surface of the electrode; in consequence, the optimum scan number of 20 should be selected.

3.5.3. pH effect

Since pH value could influence the redox response of Th and biocatalytic activity of HRP, the response of the biosensor for 1.0 pg mL^{-1} of anti-p53 autoantibody in buffer solutions with various pH values containing 2.5 mM of H_2O_2 was investigated by recording of DPV. As shown in Fig. 5C, the peak current increased with increasing pH from 4.0 to 7.0, then gradually decreased when pH increased until 9.0. The maximum response of H_2O_2 solution was observed at pH 7.0. Subsequently pH = 7 was chosen as optimum pH (0.1 M PBS) for anti-p53 autoantibody detection.

3.5.4. H_2O_2 concentration

Also, the effect of H_2O_2 concentration on the biosensor response was examined by recording DPV. As illustrated in Fig. 5D, with increasing of H $_2O_2$ concentration, the biosensor response increased and at concentration more than 2.5 mmol, a plateau level was reached. Therefore, 2.5 mmol chosen as optimal value of H_2O_2 concentration in the proposed immunosensor.

3.5.5. Incubation time

Another important parameter in the preparation of the immunosensor is incubation time for the interaction between anti-p53 autoantibody and p53-antigen as well as the interaction between anti-p53 autoantibody and HRP-conjugated secondary antibody. The peak current was amplified as the time of incubation increased in the range of 10–50 min and then remained fairly constant in the range of 50–80 min for the incubation time between anti-p53 autoantibody and p53-antigen (Fig. 5e). Similarly, with increasing incubation time, the obtained DPV current increased until 60 min and then reached a plateau, which portended a saturated binding between the anti-p53 autoantibody and HRP-conjugated secondary antibody (Fig. 5f). Based on these results, 50 and 60 min were chosen as the optimal incubation times for interaction of the anti-p53 autoantibody with p53-antigen and HRP-conjugated secondary antibody, respectively.

3.5.6. p53-antigen concentration

In order to obtain the maximum concentration of immobilized p53-antigen on the surface of the modified electrode, different concentrations of p53-antigen (5, 10, 20, 30, 40, 50, 60, 70, and 80 ng mL^{-1}) applied for immobilization on the surface of modified electrode. As shown in Fig. S5**,** the current of DPVs decrease with the increase of antigen level from 5 ng mL^{-1} till 50 ng mL^{-1}; after that, a plateau level was reached. Thus, the optimal p53-antigen concentration was selected to be 50 ng.$mL^{-1}$for the whole biosensing process.

3.6. Analytical performance of the immunosensor

Under optimal conditions, the performance of the immunoassay was examined for detecting different concentrations of anti-p53 autoantibody by two techniques (DPV and EIS). Firstly, typical DPVs of the electrochemical immunosensor in the presence of different concentrations of anti-p53 autoantibody (0.1–500 pg mL^{-1} from "a" to "n") were recorded in Fig. 6A. As illustrated in Fig. 6B, the bioelectrocatalytic currents increased with increasing anti-p53 autoantibody concentration in two linear concentration ranges. In the lower rang (0.1, 0.5, 2, 4, 6, 8, and 10 pg mL^{-1}) the regression equation derived as I(μA) = 0.4597[anti-p53 autoantibody]/pg mL^{-1}+8.2617 μA and the correlation coefficient was 0.9982. Also, the sensitivity was 0.4597 μA.pg.mL^{-1}, and limit of detection (LOD) was calculated to be 0.01 pg mL^{-1}(S/N = 3.3). At the higher range (10, 30, 60, 100, 200, 300, 400, and 500 pg ml^{-1}) the regression equation was I(μA) = 0.0001[anti-p53 autoantibody]/pg.mL^{-1}+13.304 μA (Fig. 6D). The correlation coefficient and sensitivity were found to be 0.9989 and 0.0001 μA pg.ml^{-1}, respectively. As mentioned above, the calibration curve displayed two linear range regions with different slopes. When the biosensor was utilized to detect anti-p53 autoantibodies, the amount of active sites of p53-antigen became fewer with increasing anti-p53 autoantibodies concentration. Therefore, the sensitivity declines when the biosensor is used to quantify a higher level of anti-p53 autoantibodies, and the calibration curves with two different slopes were observed. The obtained results were in good agreement with other reports for immunosensors [32,42,43].

Secondly, Nyquist complex plane plots of the biosensor in the presence of different concentrations of anti-p53 autoantibodies (5, 10, 25, 50, 75, 100, 125, and 150 pg mL^{-1}) were recorded under the optimum conditions in 0.1 M KCl solution containing 5 mM $[Fe(CN)6]^{-3/-4}$. As shown in Fig. 6E, with increasing concentration of anti-p53 autoantibodies at range (5–150 pg $mL^{-1)}$ the charge transfer resistance increased, and a linear relationship obtained between concentration and charge transfer (Fig. 6F). The regression equation was ΔR(Ω) = 6.4843 [anti-p53 autoantibody]/pg.mL^{-1}+232.93Ω. The correlation coefficient and sensitivity were found to be 0.9986 and 6.4843 Ω.pg.ml^{-1}, respectively and the estimated LOD was to be 0.02 pg mL^{-1}.

On the other hand, to further expound the amplification of the developed immunosensor toward anti-p53 autoantibody determination, the response of the proposed bioassay was compared to those of other methods in Table 1. The results in Table 1 clearly represent that the proposed strategy for anti-p53 autoantibody sensing shows better performance in some cases or comparable with the other methods reported so far.

In addition, the DPV responses of different concentrations of anti-p53 autoantibody (0.1, 1, 1.8, 3, 4, and 5 U mL^{-1}) were recorded in PBS (pH = 7.0) containing 2.5 mM H_2O_2 at the surface of the modified electrode. As projected, the peak current increased during increasing of

Table 1
Analytical parameters for different anti-p53 autoantibody biosensors.

Diagnostic device	Electrochemical technique	Concentration range	LOD	Ref.
g-G[a]-AuNP-dsDNA modified electrode	EIS	0.1 ng L^{-1} to 0.1 μg L^{-1}	0.1 pg mL^{-1}	[14]
Microcantilever	Piezoresistive effect	20 ng mL^{-1} to 20 μg mL^{-1}	Not reported	[44]
Au NPs/GO/SPCE	SWV[d]	0.1 pg mL^{-1} to 10 ng mL^{-1}	0.088 pg mL^{-1}	[1]
HaloTag-MBs[b]/ SPCE	Amperometry	1.1–5 U mL^{-1}	0.34 U mL^{-1}	[15]
Au–NPFe_2O_3NC[c]	Amperometry	0.0875–7 U mL^{-1}	0.08 U mL^{-1}	[11]
Au-PEA-SA[e]	EIS	1.0–1000 ng mL^{-1}	103 pg mL^{-1}	[45]
Th/CS/Ni $(OH)_2$NPs/ ERGO/GCE	DPV	0.1–500 pg mL^{-1}	0.001 pg mL^{-1}	This study
CS/Ni$(OH)_2$NPs/ ERGO/GCE	EIS	5–150 pg mL^{-1}	0.007 pg mL^{-1}	This study
Th/CS/Ni $(OH)_2$NPs/ ERGO/GCE	DPV	0.1–5 U mL^{-1}	0.072 U mL^{-1}	This study

[a] Glycine-graphene.
[b] Magnetic microcarriers.
[c] Gold-Loaded Nanoporous Ferric Oxide Nanocubes.
[d] Square Wave Voltammetry.
[e] Gold electrode-phenyl ethylamine-succinic acid.

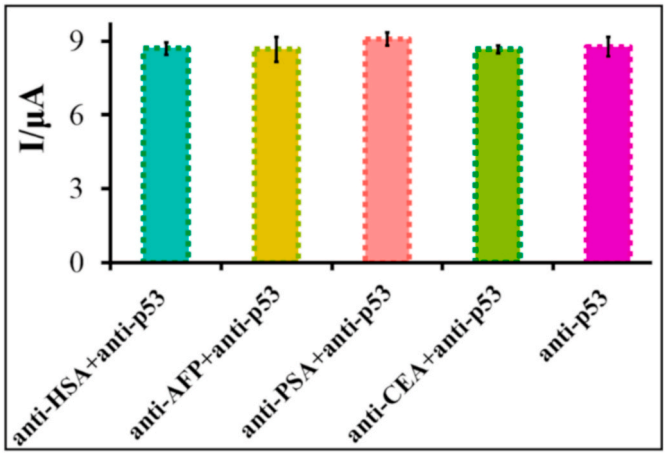

Fig. 7. The changes of DPV response after incubation with 5 pg ml^{-1} of anti-p53 autoantibody in the presence of 5 pg mL^{-1} of other antibodies (anti-HSA antibody, anti-AFP antibody, anti-PSA antibody, and anti-CEA antibody) as interference species, the electrolyte used in the cell: in 0.1 M PBS (pH = 7) containing 2.5 mM H_2O_2.

anti-p53 autoantibody level in the range of 0.1–5 U mL^{-1}. The limit of detection (LOD) calculated to be 0.072 U mL^{-1} (Fig. S6).

3.7. Reproducibility and precision of the biosensor

The reproducibility of the immunosensor was estimated by successive determination of 50 pg mL^{-1} of anti-p53 autoantibody using five biosensors under optimum experimental conditions independently. The relative standard deviation was determined to be 2.4%. Furthermore, the precision of the biosensor was evaluated by 10 repeated measuring of 50 pg mL^{-1} of anti-p53 autoantibody. The relative standard deviation was determined to be 2.6%, showing acceptable reproducibility and precision of the proposed bioassay.

3.8. Selectivity

Selectivity is an important index to obtain accurate results. Hence, the selectivity of the proposed biosensor was tested under the same experimental conditions by challenging the biosensor against 5 pg ml^{-1} of anti-p53 autoantibody in the presence of 5 pg mL^{-1} of other antibodies including anti-HSA antibody, anti-AFP antibody, anti-PSA antibody, and anti-CEA antibody as interference agents. As depicted in Fig. 7, the DPV current response was not magnified in comparison with 5 pg ml^{-1} anti-p53 antibody alone. These results demonstrated that the proposed biosensor showed good selectivity to detect the anti-p53 autoantibodies.

3.9. Application of the biosensor for anti-p53 autoantibody detection in spiked and real human serum samples

Anti-p53 autoantibodies are found predominantly in cancer-suffering patients with a specificity of 96%. Such antibodies are usually associated with *p53* gene mutations and p53-protein accumulation in the tumor, but the sensitivity of such detection is only 30% [46,47]. Thus, for detection of anti-p53 autoantibody, developing of a method with amplified sensitivity is of great interest. Regarding this issue, electrochemical biosensors can be not only a very high sensitivity but also a selectivity, simplicity, rapidness, portable, and low-cost method for analysis of various analytes such as anti-p53 autoantibodies.

Thus, the applicability of the proposed immunosensor for detection of anti-p53 autoantibody in human serum samples was evaluated. For this purpose, human serum samples were obtained from five healthy volunteers and 100-folds diluted with PBS solution (pH 7.0) before analysis without further pretreatments. The sera samples spiked with known amounts of anti-p53 antibody, and the values of analyte in serum samples detected with the proposed immunosensor and the observed recoveries (n = 3) reported in Table 2. As illustrated the recoveries for various concentration of the analyte is in the range 98–107%, so, the developed biosensor can be successfully applied for anti-p53 autoantibody quantification in real samples.

Table 2
Detection of anti-p53 autoantibody in the human serum samples under optimization conditions using DPV technique. Each measurement repeated three times (n = 3) and the mean values reported.

Serum sample No.	Added (pg. mL^{-1})	Found (pg. mL^{-1})	Recovery (%)	RSD (%)
1	1	1.07	107.00	0.76
2	5	4.89	97.80	0.80
3	50	51.30	102.60	1.06
4	100	101.23	101.23	2.13
5	300	296.15	98.70	0.65

To further evaluate the analytical reliability and possible application of the proposed immunoassay in clinical analysis, six human serum samples were collected from cancerous and healthy subjects. When the levels of anti-p53 autoantibodies were higher than the upper limit of the calibration ranges, serum samples were diluted 100 times with PBS (pH = 7.0) in order to obtain responses in the linear range of the proposed method. As reported in the literature [46,47], in the serum of healthy subjects, the presence of anti-p53 autoantibody is extremely rare (Fig. S7). However, anti-p53 autoantibody was detected in sera from cancerous subjects over the range 1.76–3.60 U mL^{-1} and less than 0.03 U mL^{-1} for negative serum samples (in the case of 100 times diluted samples). It means 176–360 U mL^{-1} that is upper than the cut off (120 U mL^{-1}) and the values less than 3 U mL^{-1} in the case of undiluted serum samples of them. The experimental results were summarized in Table S1.

4. Conclusion

A novel and simple electrochemical biosensor was designed and validated for the detection of anti-p53 autoantibody. The methodology, involving the use of CS/$Ni(OH)_2$NPs/ERGO as a promising transduction platform for covalent attachment of p53-antigen and Th onto the platform and also HRP-conjugated secondary antibody for signal amplification and H_2O_2 as the substrate. The immunosensor exhibits an excellent performance for providing p53 autoantibodies detection, which might serve to monitor patient levels of p53 autoantibodies during the course of cancer monitoring or therapeutic manipulating. The enhanced sensitivity of the immunoassay was mainly due to the large surface area of the platform that facilitated the binding of increased amount of covalently attached p53-antigen and hence improvement of electrocatalytic activity of Th/HRP system toward H_2O_2 reduction signal. Under optimized condition, the conducted immunoassay successfully detected the p53 autoantibodies in diluted serum using DPV and EIS as a label free analytical technique. The as-prepared biosensor displayed satisfactory sensitivity, stability, simplicity, reproducibility, rapidness and specificity for anti-p53 autoantibody detection. The proposed strategy can be developed as effective process for immunosensor fabrication bio devices design and their application in biosensing and clinical diagnostics.

Declaration of competing interest

The authors declare that they have no known competing financial interests or personal relationships that could have appeared to influence the work reported in this paper.

Acknowledgments

The authors wish to thank Tehran University of Medical Sciences, Tehran, Iran for the financial and instrumental support of this study.

Appendix A. Supplementary data

Supplementary data to this article can be found online at https://doi.org/10.1016/j.talanta.2021.122276.

Credit roles

Bahareh Feyzi-barnaji: Investigation, Conceptualization, Writing – original draft, Rassoul Dinarvand: Supervision, Funding acquisition, Resources, Hamid Salehzadeh: Validation, Editing, Elham Arkan: Formal analysis, Abdollah Salimi: Methodology, Editing, Fatemeh Nili: Resources, Ali Mohammadi: Supervision, Methodology, Reviewing and Editing.

References

[1] R. Elshafey, M. Siaj, A.C. Tavares, Au nanoparticle decorated graphene nanosheets for electrochemical immunosensing of p53 antibodies for cancer prognosis, Analyst 141 (9) (2016) 2733–2740.
[2] B. Sadikovic, K. Al-Romaih, J. Squire, M. Zielenska, Cause and consequences of genetic and epigenetic alterations in human cancer, Curr. Genom. 9 (6) (2008) 394–408.
[3] M.M. Atta, S.A. El-Masry, M. Abdel-Hameed, H.A. Baiomy, N.E. Ramadan, Value of serum anti-p53 antibodies as a prognostic factor in Egyptian patients with hepatocellular carcinoma, Clin. Biochem. 41 (14–15) (2008) 1131–1139.
[4] K.S. Anderson, J. Wong, A. Vitonis, C.P. Crum, P.M. Sluss, J. LaBaer, et al., p53 autoantibodies as potential detection and prognostic biomarkers in serous ovarian cancer, Cancer Epidemiol. Biomark. Prev. 19 (3) (2010) 859–868.
[5] L. Crawford, D. Pim, R. Bulbrook, Detection of antibodies against the cellular protein p53 in sera from patients with breast cancer, Int. J. Canc. 30 (4) (1982) 403–408.
[6] M. Cioffi, M.T. Vietri, P. Gazzerro, R. Magnetta, A. D'Auria, A. Durante, et al., Serum anti-p53 antibodies in lung cancer: comparison with established tumor markers, Lung Canc. 33 (2–3) (2001) 163–169.
[7] C. Tan, X. Qian, Z. Guan, B. Yang, Y. Ge, F. Wang, et al., Potential biomarkers for esophageal cancer, SpringerPlus 5 (1) (2016) 467.
[8] J.-M. Portefaix, C. Fanutti, C. Granier, E. Crapez, R. Perham, J. Grenier, et al., Detection of anti-p53 antibodies by ELISA using p53 synthetic or phage-displayed peptides, J. Immunol. Methods 259 (1–2) (2002) 65–75.
[9] G. Yan, D. Xing, S. Tan, Q. Chen, Rapid and sensitive immunomagnetic-electrochemiluminescent detection of p53 antibodies in human serum, J. Immunol. Methods 288 (1–2) (2004) 47–54.
[10] B. Mudenda, J. Green, B. Green, J. Jenkins, L. Robertson, M. Tarunina, et al., The relationship between serum p53 autoantibodies and characteristics of human breast cancer, Br. J. Canc. 69 (6) (1994) 1115–1119.
[11] M.K. Masud, S. Yadav, M.N. Islam, N.-T. Nguyen, C. Salomon, R. Kline, et al., Gold-loaded nanoporous ferric oxide nanocubes with peroxidase-mimicking activity for electrocatalytic and colorimetric detection of autoantibody, Anal. Chem. 89 (20) (2017) 11005–11013.
[12] M. Labib, E.H. Sargent, S.O. Kelley, Electrochemical methods for the analysis of clinically relevant biomolecules, Chem. Rev. 116 (16) (2016) 9001–9090.
[13] E. Prats-Alfonso, X. Sisquella, N. Zine, G. Gabriel, A. Guimerà, F.J. Del Campo, et al., Cancer prognostics by direct detection of p53-antibodies on gold surfaces by impedance measurements, Small 8 (13) (2012) 2106–2115.
[14] H. Imran, P.N. Manikandan, D. Prabhu, V. Dharuman, J. Jeyakanthan, J.H. Hahn, Ultra selective label free electrochemical detection of cancer prognostic p53-antibody at DNA functionalized graphene, Sens Biosensing Res 23 (1) (2019) 100261.
[15] M. Garranzo-Asensio, A. Guzman-Aranguez, C. Povés, M.J. Fernández-Aceñero, R. M. Torrente-Rodríguez, V. Ruiz-Valdepeñas Montiel, et al., Toward liquid biopsy: determination of the humoral immune response in cancer patients using halotag fusion protein-modified electrochemical bioplatforms, Anal. Chem. 88 (24) (2016) 12339–12345.
[16] N. Wongkaew, M. Simsek, C. Griesche, A.J. Baeumner, Functional nanomaterials and nanostructures enhancing electrochemical biosensors and lab-on-a-chip performances: recent progress, applications, and future perspective, Chem. Rev. 119 (1) (2018) 120–194.
[17] M. Sharifi, M.R. Avadi, F. Attar, F. Dashtestani, H. Ghorchian, S.M. Rezayat, et al., Cancer diagnosis using nanomaterials based electrochemical nanobiosensors, Biosens. Bioelectron. 126 (1) (2019) 773–784.
[18] N. Özcan, C. Karaman, N. Atar, O. Karaman, M.L. Yola, A novel molecularly imprinting biosensor including graphene quantum dots/multi-walled carbon nanotubes composite for interleukin-6 detection and electrochemical biosensor validation, ECS J. Solid State Sci. Technol. 9 (12) (2020) 121010.
[19] V. Velusamy, S. Palanisamy, S.-W. Chen, S. Balu, T.C. Yang, C.E. Banks, Novel electrochemical synthesis of cellulose microfiber entrapped reduced graphene oxide: a sensitive electrochemical assay for detection of fenitrothion organophosphorus pesticide, Talanta 192 (2019) 471–477.
[20] K.-C. Mei, N. Rubio, P.M. Costa, H. Kafa, V. Abbate, F. Festy, et al., Synthesis of double-clickable functionalised graphene oxide for biological applications, ChemComm 51 (81) (2015) 14981–14984.
[21] V.K. Gupta, M.L. Yola, M.S. Qureshi, A.O. Solak, N. Atar, Z. Üstündağ, A novel impedimetric biosensor based on graphene oxide/gold nanoplatform for detection of DNA arrays, Sensor. Actuator. B Chem. 188 (2013) 1201–1211.
[22] M.L. Yola, Electrochemical activity enhancement of monodisperse boron nitride quantum dots on graphene oxide: its application for simultaneous detection of organophosphate pesticides in real samples, J. Mol. Liq. 1 (277) (2019) 50–57.
[23] G.B. Gizem, H. Medetalibeyoglu, N. Atar, M.L. Yola, Efficient direct-methanol fuel cell based on graphene quantum dots/multi-walled carbon nanotubes composite, Electroanalysis 32 (9) (2020) 1977–1982.
[24] N. Atar, T. Eren, M.L. Yola, H. Gerengi, S. Wang, Fe@ Ag nanoparticles decorated reduced graphene oxide as ultrahigh capacity anode material for lithium-ion battery, Ionics 21 (12) (2015) 3185–3192.
[25] M.L. Yola, N. Atar, A.(P.E.A. Phenylethanolamine, Imprinted polymer on carbon nitride nanotubes/graphene quantum dots/core-shell nanoparticle composite for electrochemical PEA detection in urine sample, J. Electrochem. Soc. 165 (2) (2018).
[26] R. Wang, J. Lang, Y. Liu, Z. Lin, X. Yan, Ultra-small, size-controlled Ni(OH)2 nanoparticles: elucidating the relationship between particle size and electrochemical performance for advanced energy storage devices, NPG Asia Mater. 7 (6) (2015).
[27] Y. Xing, H. Lin, D. Cao, Q. Xu, W. Han, R. Wang, et al., Effect of chitosan coating with cinnamon oil on the quality and physiological attributes of China jujube fruits, BioMed Res. Int. 2015 (2015).
[28] F.G. Ortega, S.V. Piguillem, G.A. Messina, G.R. Tortella, O. Rubilar, M.I. Castillo, J. A. Lorente, M.J. Serrano, J. Raba, M.A. Baldo, EGFR detection in extracellular vesicles of breast cancer patients through immunosensor based on silica-chitosan nanoplatform, Talanta 194 (2019) 243–252.
[29] S. Khezrian, A. Salimi, H. Teymourian, R. Hallaj, Label-free electrochemical IgE aptasensor based on covalent attachment of aptamer onto multiwalled carbon nanotubes/ionic liquid/chitosan nanocomposite modified electrode, Biosens. Bioelectron. 43 (2013) 218–225.
[30] A. Adumitrăchioaie, M. Tertiș, M. Suciu, F. Graur, C. Cristea, A novel immunosensing platform for serotonin detection in complex real samples based on graphene oxide and chitosan, Electrochim. Acta 311 (10) (2019) 50–61.
[31] J. Choosang, S. Khumngern, P. Thavarungkul, P. Kanatharana, A. Numnuam, An Ultrasensitive Label-free Electrochemical Immunosensor Based on 3D Porous Chitosan–Graphene–Ionic Liquid–Ferrocene Nanocomposite Cryogel Decorated with Gold Nanoparticles for Prostate-specific Antigen, Talanta, 2020, p. 121787.
[32] B. Kavosi, A. Salimi, R. Hallaj, K. Amani, A highly sensitive prostate-specific antigen immunosensor based on gold nanoparticles/PAMAM dendrimer loaded on MWCNTS/chitosan/ionic liquid nanocomposite, Biosens. Bioelectron. 52 (15) (2014) 20–28.
[33] C. Natarajan, H. Matsumoto, G. Nogami, Improvement in electrochromic stability of electrodeposited nickel hydroxide thin film, J. Electrochem. Soc. 144 (1) (1997) 121.
[34] S. Rastgar, S. Shahrokhian, Nickel hydroxide nanoparticles-reduced graphene oxide nanosheets film: layer-by-layer electrochemical preparation, characterization and rifampicin sensory application, Talanta 119 (2014) 156–163.
[35] B. Feyzi-barnaji, B. Darbasizadeh, E. Arkan, H. Salehzadeh, A. Salimi, F. Nili, et al., Immunoreaction-triggered diagnostic device using reduced graphene oxide/CuO NPs/chitosan ternary nanocomposite, toward enhanced electrochemical detection of albumin, J. Electroanal. Chem. 877 (2020) 114642.
[36] A. Salimi, B. Kavosi, F. Fathi, R. Hallaj, Highly sensitive immunosensing of prostate-specific antigen based on ionic liquid–carbon nanotubes modified electrode: application as cancer biomarker for prostatebiopsies, Biosens. Bioelectron. 42 (2013) 439–446.
[37] L.A. Hutton, M. Vidotti, A.N. Patel, M.E. Newton, P.R. Unwin, J.V. Macpherson, Electrodeposition of nickel hydroxide nanoparticles on boron-doped diamond electrodes for oxidative electrocatalysis, J. Phys. Chem. C 115 (2011) 1649–1658.
[38] E. Laviron, General expression of the linear potential sweep voltammogram in the case of diffusionless electrochemical systems, J. Electroanal. Chem. 101 (1) (1979) 19–28.
[39] Z. Biniaz, A. Mostafavi, T. Shamspur, M. Torkzadeh-Mahani, M. Mohamadi, Electrochemical sandwich immunoassay for the prostate specific antigen using a polyclonal antibody conjugated to thionine and horseradish peroxidase, Microchim. Acta 184 (8) (2017) 2731–2738.
[40] P.E. Erden, E. Kılıç, A review of enzymatic uric acid biosensors based on amperometric detection, Talanta 107 (30) (2013) 312–323.
[41] H. Chen, D. Luo, B. Shang, J. Cao, J. Wei, Q. Chen, et al., Immunoassay-type biosensor based on magnetic nanoparticle capture and the fluorescence signal formed by horseradish peroxidase catalysis for tumor-related exosome determination, Microchim. Acta 187 (2020) 1–8.
[42] Z. Dai, J. Chen, F. Yan, H. Ju, Electrochemical sensor for immunoassay of carcinoembryonic antigen based on thionine monolayer modified gold electrode, Canc. Detect. Prev. 29 (3) (2005) 233–240.
[43] Y. Yuan, R. Yuan, Y. Chai, Y. Zhuo, Y. Shi, X. He, et al., A reagentless amperometric immunosensor for alpha-fetoprotein based on gold nanoparticles/TiO2 colloids/prussian blue modified platinum electrode, Electroanalysis 19 (2) (2007) 1402–1410.

[44] Y. Zhou, Z. Wang, W. Yue, K. Tang, W. Ruan, Q. Zhang, et al., Label-Free detection of p53 antibody using a microcantilever biosensor with piezoresistive readout, Sensors IEEE2009 (2009) 819–822.
[45] O.K. Adeniyi, P.N. Mashazi, Stable thin films of human P53 antigen on gold surface for the detection of tumour associated anti-P53 autoantibodies, Electrochim. Acta 331 (2020) 135272.
[46] T. Soussi, p53 Antibodies in the sera of patients with various types of cancer: a review, Canc. Res. 60 (7) (2000) 1777–1788.
[47] P. Pan, Y. Wang, Y. Zhu, X. Gao, Z. Ju, P. Qiu, L. Wang, C. Mao, Nontoxic virus nanofibers improve the detection sensitivity for the anti-p53 antibody, a biomarker in cancer patients, Nano Res 8 (11) (2015) 3562–3570.